Vertex Climax: Converting Geometry into a Non-nanifold Midsurface

Christoph Schinko[1,2] and Torsten Ullrich[1,2][a]
[1]Fraunhofer Austria Research GmbH, Graz, Austria
[2]Technische Universität Graz, Graz, Austria

Keywords: Midsurface, Grid-based Algorithm, Volume Graphics, Design Automation.

Abstract: The physical simulation of CAD models is usually performed using the finite elements method (FEM). If the input CAD model has one dimension that is significantly smaller than its other dimensions, it is possible to perform the physical simulation using thin shells only. While thin shells offer an enormous speed-up in any simulation, the conversion of an arbitrary CAD model into a thin shell representation is extremely difficult due to its non-uniqueness and its dependence on the simulation method used afterwards. The current state-of-the-art algorithms in conversion voxelize the input geometry and remove voxels based on matched, predefined local neighborhood configurations until only one layer of voxels remains.

In this article we discuss a new approach that can extract a midsurface of a thin solid using a kernel-based approach: In contrast to other voxel-based thinning approaches, our algorithm applies a kernel onto a binary grid. In the resulting density field, opposing surface-voxels are iteratively moved towards each other until a thin representation is obtained.

1 INTRODUCTION

The analysis of thin-walled parts is a discipline of Computer-Aided Engineering (CAE) analysis. As physical simulations are computationally costly, they benefit from reduced-complexity representations, so called “Midsurfaces” (Kulkarni, 2016). The reduction in complexity is achieved by replacing such Computer-Aided Design (CAD) models with a simplified model consisting of non-manifold 2D-surfaces lying (mostly) midway of the original walls.

Midsurfaces are part of the larger family of medial objects. A common member of this family is the medial axis.

Definition: The *medial axis* (also called medial surface) of a closed object is the set of centers of empty spheres which touch the surface of the object at more than one point.

Another member of the family of medial objects is the straight skeleton. The straight skeleton is defined only for polygons and has been introduced by O. AICHHOLZER and F. AURENHAMMER (Aichholzer and Aurenhammer, 1996). In contrast to the medial axis it consists only of line segments (see Figure 1). The straight skeleton is defined by a shrinking process of the polygon. The edges of the polygon are moved inwards in a self-parallel manner and at the same speed. When all parts have shrunken to zero, the process terminates. The straight skeleton now consists of the paths drawn by the polygon vertices during the shrinking process. The result can be seen as a variant of the medial axis, because, in the case of convex polygons, both structures are identical (Demuth and Aurenhammer, 2010).

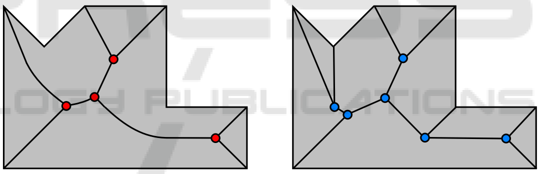

Figure 1: The medial axis of some input geometry consists of all points that are the center of a sphere which touches the input at more than one point (left). The straight skeleton is the result of a shrinking process returning a graph structure of line segments only (right).

Both, the definition of a medial axis as well as the definition of the straight skeleton, only depend on the input object. By contrast, the midsurface definition not only depends on the input, but also on the output of a subsequent analysis:

Definition: The *midsurface* of a closed, thin-walled object is a set of non-manifold surfaces which reveal in a CAE analysis the same results (within a δ-

[a] https://orcid.org/0000-0002-7866-9762

Schinko, C. and Ullrich, T.
Vertex Climax: Converting Geometry into a Non-nanifold Midsurface.
DOI: 10.5220/0010210401850192
In *Proceedings of the 16th International Joint Conference on Computer Vision, Imaging and Computer Graphics Theory and Applications (VISIGRAPP 2021) - Volume 1: GRAPP*, pages 185-192
ISBN: 978-989-758-488-6

tolerance) as the closed, thin-walled input model.

Therefore, any statements regarding the correctness of a midsurface transformation can only be validated within a specific context. A possible difference between the results of both transformation types is illustrated in 2D in Figure 2.

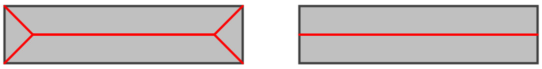

Figure 2: The result of a medial axis transformation (left) and the midsurface transformation of a thin-walled part (grey) are usually different. As the midsurface has to respect follow-up simulation usages, both results (left & right) may be a correct midsurface depending on the application context.

This article presents a novel voxel-based midsurface generation approach for thin-walled objects; the first, preliminary sketch of this algorithm has been presented in a poster session at the Fabrication & Sculpting Event (FASE) at Shape Modeling International (SMI) 2020 (Schinko and Ullrich, 2020). In contrast to the preliminary sketch, a detailed description and a thorough evaluation have been added to this article.

2 RELATED WORK

Related work in the area of midsurface generation for solid geometries can be divided into surface-based approaches and grid-based (so-called thinning) approaches.

H. LOCKETT and M. GUENOV address the difficulty in finding similarity measures for evaluating the quality of midsurface models (Lockett and Guenov, 2008). Without a ground truth, the proposed methods perform a geometric and topological comparison between the midsurface models and their solid counterparts. A global measure of geometric similarity is based on the Hausdorff distance (Ullrich et al., 2008) and defines the proportion of solid model points that are within a specified threshold distance of the midsurface model. For measuring the global topological similarity, geometry graph attributes are used. Both measures can be combined into an overall similarity index to provide interesting insights.

2.1 Top-down

The group of top-down approaches are surface-based approaches working on boundary representations (Schinko et al., 2017). A divide and conquer strategy simplifies the transformation into midsurfaces by splitting complex parts into smaller sub-parts according to semantic interrelationships (Sun et al., 2016). This kind of approach is also used by Y. H. WOO and C. U. CHOO (Woo and Choo, 2009). They decompose a solid model into simple volumes and generate midsurfaces using an existing algorithm based on face-pairs (the top and the bottom side of a thin layer are called face-pairs or corresponding faces (Rezayat, 1996); in a boundary representation these faces usually don't have any explicit correspondence).

In their work, NOLAN et al. rely on feature detection to assign mixed-dimensional finite element models to three categories: complex regions, long-slender regions, and thin-sheet regions (Nolan et al., 2014). Relations between the original solid model and the dimensionally reduced version are maintained.

In the area of surface-based midsurface generation, the state-of-the-art approaches for decomposition (Kulkarni et al., 2017b), identification of corresponding faces (Kulkarni and Kale, 2014), and a divide and conquer strategy (Kulkarni et al., 2017a) have been presented by Y. H. KULKARNI: "Development of Algorithms for Generating Connected Midsurfaces using Feature Information in Thin-Walled Parts" (Kulkarni, 2016).

2.2 Bottom-up

Due to the nature of our approach being grid-based, this Section focuses on a subgroup of so-called thinning approaches. The idea behind these approaches is to iteratively shrink an object locally by offsetting its boundary towards its interior. This process is stopped, when the interior vanishes and just a (usually non-manifold) surface structure remains. Like our approach, many thinning approaches work on binary voxels, a concept attributed to the field of digital topology. Early work in this field dates back to the late 1960s and is surveyed by T.Y KONG and A. ROSENFELD (Kong and Rosenfeld, 1989). A good description of toplogical structures of voxels and concepts like neighborhood, connectivity and Euler number is given by J. TORIWAKI and T. YONEKURA (Toriwaki and Yonekura, 2002). Their work also introduces new local features to study the effect of deleting 1-voxels – a fundamental process during thinning.

Thinning approaches have a long history: P. KWOK and V. RANJAN give a good overview of the most important thinning algorithms up to 1991 (Kwok and Ranjan, 1991). All presented algorithms work on voxel data and eventually result in a skeleton rather than a surface. Another volume thinning method for generating a skeleton that can be used in searching for intersected cells in isosurface propagation is presented by ITOH et al. (Itoh et al., 1996). Their graph-based approach connects all extremum points of a volume to a one-cell wide skeleton and contains its topological features. S. PROHASKA and H.-C. HEGE propose a robust, noise resistant criterion for the characterization of plane-like skeletons (Prohaska and Hege, 2002). Their algorithm uses the geodesic distance along the object's boundary and a distance map. After obtaining a skeleton of lines and surfaces, the focus is on obtaining a surface representation for expressive rendering of complex structures.

In contrast to the already mentioned algorithms that return skeletons, the work by T.-C. LEE and R. L. KASHYAP on thinning algorithms is concerned with parallel thinning for extracting medial surfaces and medial axes of binary voxel data (Lee and Kashyap, 1994). The algorithm uses the Euler characteristic to preserve topological properties of binary voxel data during the thinning process. Another thinning algorithm for extracting medial surfaces is presented by C.-M. MA and S.-Y. WAN (Ma and Wan, 2001). It defines two sets of voxels on the grid: one consisting of the 26-neighborhood of all 1-voxels and one consisting of the 6-neighborhood of all 0-voxels. The algorithm alternatively works on the two sets deleting all possible 1-voxels, and terminates when no 1-voxels can be deleted anymore. It is proven to preserve connectivity.

The work of FUJIMORI et al. focuses on extracting separated medial surfaces (Fujimori et al., 2006). Medial surfaces are obtained by classifying voxels into medial surface voxels using geodesic distances along all three axes. Connected regions are separated by using the average thickness as an indicator (a constant thickness of all parts is assumed). The separation is performed by offsetting them into the direction of the object surface. In a final step, a polygonal surface is extracted using a marching cubes approach. Another thinning approach for medial surface extraction is presented by K. PALÁGYI and G. NÉMETH (Palágyi and Németh, 2009). The proposed algorithms rely on sufficient conditions for parallel, topology-preserving reduction operators. A novel thinning scheme using iteration-level endpoint checking is proposed in follow-up work (Németh et al., 2010).

2.3 Surface Reconstruction

Using a grid-based data structure for thinning, our approach has to convert the remaining voxels representing the midsurface into a polygonal, non-manifold representation. An important algorithm to extract a polygonal representation of an isosurface within a three-dimensional, discrete scalar field is the well-known *marching cubes* algorithm by W. E. LORENSEN and H. E. CLINE (Lorensen and Cline, 1987). It is in the nature of the marching cubes algorithm to produce a dense triangulation (even on flat surfaces) and voxel *artifacts*. In case normal information is available for each voxel, surface reconstruction algorithms are able to produce a much smoother mesh (Ju et al., 2002). Another approach is presented by KAZHDAN et al. showing that surface reconstruction of Hermite data can be formulated as a Poisson problem (Kazhdan et al., 2006). The algorithm reconstructs a watertight triangulation of the surface of a model.While all these algorithms produce a closed surface for all connected regions of voxels, they are not suitable for midsurface reconstruction due to its non-manifold nature (without volume and orientation). Q. T. NGUYEN and A. J. P. GOMES propose an algorithm for triangulating non-manifold implicit surfaces (Nguyen and Gomes, 2016). The idea is to leverage data generated by marching cubes and to “heal” the triangulation inside so-called critical cubes. Additional work on polygonizing non-manifold implicit surfaces is presented by YAMAZAKI et al. (Yamzaki et al., 2002). By allowing discontinuity of the field function, the proposed method yields a non-manifold surface exhibiting features like holes and boundaries. Another approach to reconstruct medial surfaces from volumetric data of thin-plate objects is presented by T. MICHIKAWA and H. SUZUKI (Michikawa and Suzuki, 2010). Their algorithm is based on distance fields of binary volumes and uses spherical support to build correct junctions where conventional approaches produce small cavities.

As the result of all midsurface generation algorithms require manual inspection and corrections, the manual and the automatic creation of a midsurface still cause a similar effort.

3 VERTEX CLIMAX

Our new grid-based approach consists of four steps, which are described shortly to give an overview, and which are illustrated in the Figures 3 and 4. The first step builds a binary 3D grid (see Figure 3, left) and marks each voxel (light red) that contains some part of the input surface geometry (dark red).

The second step interprets the binary grid as a density field with the previous markup as initial 0.0 resp. 1.0 values and applies a kernel Σ to it. In Figure 3 (right) the kernel is a simple counter (light red) that sums the values of each 3×3 neighborhood N^9. The illustration shows the color-coded result.

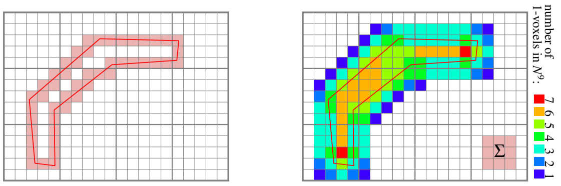

Figure 3: The new “vertex climax” algorithm determines the midsurface of a geometric model. In the first step (left) the input surface geometry is rasterized into a voxel representation. Having rasterized the input surface geometry in binary voxels, an accumulation kernel Σ transforms the binary voxels into a density field (right).

In the third step (see Figure 4, left), the vertices of the original input data are moved within the density field towards the climax (black arrows in the color coded grid).

Finally, vertices which approach each other are clustered and merged (see grey circles in Figure 4). Having merged all clusters of vertices, the resulting two-sided, incident surfaces are merged to one-sided surfaces. The result is a midsurface.

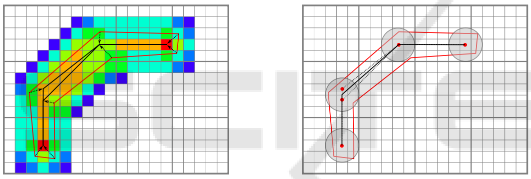

Figure 4: The accumulated density field defines a direction: The vertices of the input surface geometry are moved towards the density climax (left). The merge step (right) is performed by a mean-shift clustering algorithm (illustrated by grey circles). While merging the vertices, the surfaces (top and bottom of a geometry; dotted lines) merge as well (black line).

3.1 Rasterization Step

The *Vertex Climax* algorithm can be applied to triangle meshes only. This prerequisite is not a limitation as most CAD systems offer the possibility to export the tessellated geometry.Besides the tessellated geometry the algorithm needs two additional values: ε and δ, which are the smallest / greatest distance between two opposite surfaces that should be merged to one midsurface. All other subsequent parameters (see Table 2) are set automatically and do not need to be modified.

The first step builds a binary 3D grid and marks each voxel that has a non-empty intersection with the input surface geometry (Ogayar-Anguita et al., 2020). If the grid size α, i.e. the edge length of each cube in the voxel grid, is not specified, the algorithm uses the default value $\alpha = \frac{1}{2}\varepsilon$.

3.2 Voxel Kernel

The second step interprets the binary grid as a density field with the values 0.0, if a voxel does not contain any geometry, and 1.0 otherwise. The main idea of the second step is to spread the density values using a kernel. The overlaps of the kernels at the position of the midsurface result in significantly higher values compared to their neighborhood.

The vertex climax uses a uniform distribution over a 3D sphere with radius κ. The implementation simply sums for each voxel (i, j, k) the values of all surrounding voxels (r, s, t) with an Euclidean distance less than κ between the voxels' centers. Although many computer vision algorithms use other metrics, the Euclidean distance was chosen because it best corresponds to the approach of a manual midsurface construction, which is the blueprint for this algorithm.

3.3 Vertex Climax

In the third step, the vertices of the original input tessellation data are moved within the density field generated in the previous steps. The start position of a moving vertex is the center of its corresponding voxel. Then each vertex moves to the center of a neighboring voxel with the highest density until

1. no improvement concerning density values is possible or
2. the length of the movement path exceeds the greatest distance δ between two opposite surfaces that should be merged to one midsurface.

3.4 Vertex Clustering & Topological Cleaning

Having moved all vertices, the resulting set of vertices is clustered using a mean-shift clustering algorithm with a window size ω (with default value δ). The result is already a two-sided midsurface, in which each part is represented by two incident surfaces. As a one-sided midsurface representation is desired (the goal is as little geometry as possible), a dense resampling of the two-sided midsurface and a reconstruction according to SHAWN and WATSON (Shawn and Watson, 2011) returns the desired result.

4 EVALUATION

In order to evaluate the “Vertex Climax” algorithm, we created five geometric configurations and applied the new algorithm to them. The first data set consists of two penetrating sheet metal parts of different size and thickness, one of which is bent at one end. The second data set consists of two pipes with different diameters and wall thicknesses. The arrangement is an acute-angled T-construction where the pipe with the larger diameter is continuous. The third data set consists of a widening U-shaped beam connected to a pipe at a top outlet. The fourth configuration consists of a bent sheet metal on which two pipes are aligned at acute angles, i.e. the sheet metal is not penetrated and the pipes are not continuous. The last data set is a laser-scanned part which contains noise and which does not meet the thin-solid requirements.

Table 1 illustrates each input data set and lists their geometric properties; i.e. the number of triangles, the size of the axis-aligned bounding box Δ AABB, the smallest distance ε and the greatest distance δ between two opposite surfaces that should be merged to one midsurface. Please note, that the last data set is not a thin solid. The measured values ε and δ refer only to the parts that fulfill the thin-solid condition.

All evaluations of the “Vertex Climax” algorithm use the heuristics of the default values (see Table 2). No additional adjustment has been made. As a consequence, having measured the geometric sizes ε and δ, the algorithm runs fully automatically and requires no user interaction.

4.1 Intermediate Steps

For thin-solid input geometry, vertex climax and vertex clustering are the most time consuming steps (see Table 3). When the thin-solid condition is violated and a significant amount of grid cells is occupied, the accumulation step contributes most to the overall runtime of the algorithm.

Using the default values for the grid size, the resulting grids vary between 0.2×10^6 cells and 50.7×10^6 cells (for data set #2 and #3, respectively). Of all data sets, between 0.1×10^6 and 12.6×10^6 cells are occupied; i.e. between 19% upto 55% of all cells are nonempty.

Figure 5 shows some intermediate results of the rasterization and the subsequently applied kernel. In order to have a better view on the results of the kernel, each cell is rendered as a cube that is smaller than the cell size; additionally, the volume is clipped in the middle.

4.2 Geometric Distance

The vertex movement within the density field is limited by a maximum path length, which is the greatest thickness δ. In combination with the mean-shift-clustering, which is limited by the window size ω, the Hausdorff distance (Ullrich et al., 2008) between the input surface geometry and the resulting midsurface is expected to be at the same level. In the geometric analysis listed in Table 4, the vertex movement including vertex clustering corresponds to the one-sided distance of an actual-target-comparison (Schinko et al., 2011). Its values (average ± standard-deviation per vertex) should be ap-

Table 1: The input data sets represent geometric configurations commonly used in computer-aided geometric design. Please note that in contrast to the data sets #1 – #4, the data set #5 is not a thin solid. It has been included to demonstrate limitations.

	data set statistics	
data set #1	# elements	84 triangles
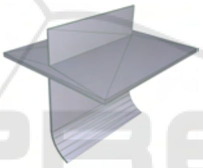	AABB	
	Δ x	149.416
	Δ y	174.837
	Δ z	155.954
	ε	1.77
	δ	4.84
data set #2	# elements	360 triangles
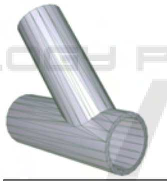	AABB	
	Δ x	63.6580
	Δ y	167.720
	Δ z	172.135
	ε	4.46
	δ	5.22
data set #3	# elements	524 triangles
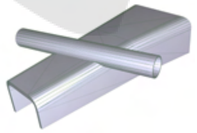	AABB	
	Δ x	263.307
	Δ y	76.1719
	Δ z	212.861
	ε	0.98
	δ	5.65
data set #4	# elements	388 triangles
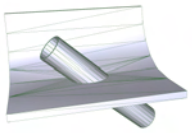	AABB	
	Δ x	139.035
	Δ y	158.949
	Δ z	123.290
	ε	1.51
	δ	6.90
data set #5	# elements	20088 triangles
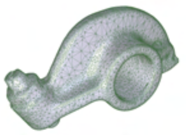	AABB	
	Δ x	2.38100
	Δ y	4.04000
	Δ z	7.84600
	ε	0.35
	δ	[0.60] (thin solid parts only)

Table 2: The default parameter settings of the vertex climax algorithm do not need to be modified in most application cases.

parameter	**default value**	**semantic**
ε	–	smallest thickness; i.e. the smallest distance between two opposite surfaces that should be merged to one midsurface
δ	–	greatest thickness; i.e. the greatest distance between two opposite surfaces that should be merged to one midsurface
α	$\frac{1}{2}\varepsilon$	grid size; i.e. the edge length of each cube in the voxel grid
κ	$\frac{3}{2}\delta$	kernel radius; i.e. the support radius of the uniform, spherical kernel
ω	δ	window size of the mean shift clustering algorithm

Table 3: The algorithm consists of four steps (rasterization, accumulation, vertex climax and vertex clustering). For thin-solid input data sets, vertex climax and vertex clustering are the most resource demanding steps of the algoritm.

data set	#1	#2	#3	#4	#5
runtime [s]					
step #1	0.01	0.01	0.01	0.01	23.20
step #2	0.01	0.01	0.01	0.01	2226.83
step #3	16.84	1.04	162.70	27.02	28.61
step #4	11.09	0.83	97.64	17.01	16.38
total	27.95	1.89	260.36	44.05	2295.02

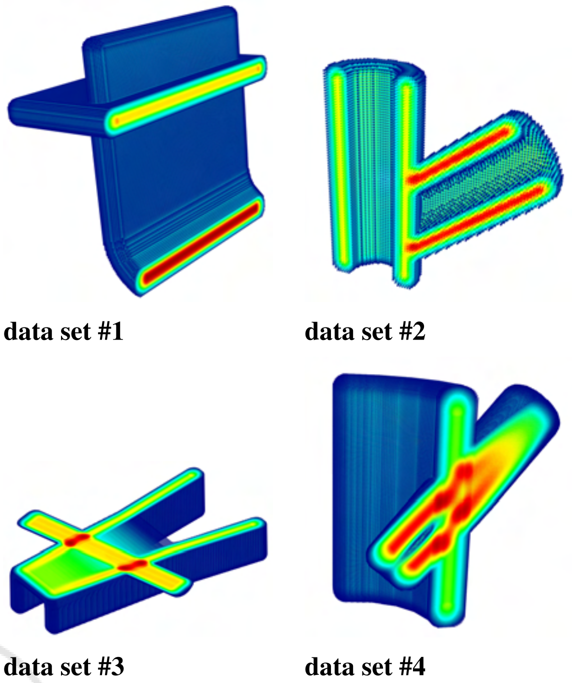

Figure 5: The main idea behind using a kernel is to spread the density values. The overlaps of the kernels at the position of the midsurface result in significantly higher values compared to their neighborhood.

Table 4: The characteristic attributes of the input surface geometry (length of the diagonal of the axis-aligned bounding box, smallest thickness ε, and greatest thickness δ) allow a quantitative comparison of input surface geometry and resulting midsurface using the average displacement of vertices and triangles during the vertex climax and vertex clustering steps. The overall comparison is quantified by the Hausdorff distance.

data set	#1	#2	#3	#4	#5
∅ AABB	277.875	248.622	347.048	244.532	9.141
ε	1.770	4.460	0.980	1.510	0.350
δ	4.840	5.220	5.650	6.900	[0.60]
one-sided distance (avg)	1.912	1.767	1.512	1.552	0.250
(± std)	0.793	1.253	1.182	1.615	0.087
Hausdorff	4.257	5.412	5.039	5.400	0.502

proximately in the range between ε and δ. Table 4 confirms these expectations for the data sets.

4.3 Final Midsurfaces

The geometric distance analysis can only detect gross errors. As a consequence, the quality of the resulting midsurfaces has been inspected and evaluated manually by several engineers with experience in construction and simulation. Figure 6 shows the input data sets (wire frame in blue) and the corresponding midsurfaces (in green) of the data sets #1 to #4. The results fully meet the requirements for midsurfaces.

Nevertheless, a minor problem exist: The limited precision is based on the grid-based approach and its cell size; but this problem can be solved at the expense of resources (memory and time).

The example data set #5, which is not a thin solid, provides interesting insights into how the algorithm works (see Figure 7). As the input data set contains holes and is not manifold, the resulting midsurface contains holes as well. Due to the grid-based rounding and the vertex clustering, the effects are intensifying and the size of the holes increases. In areas which do not meet the thin solid criteria, the density field does not reveal a consistent directional field. Therefore, the vertex movements within the density field result in self-intersections, which cannot always be cleared by the mean-shift clustering algorithm.

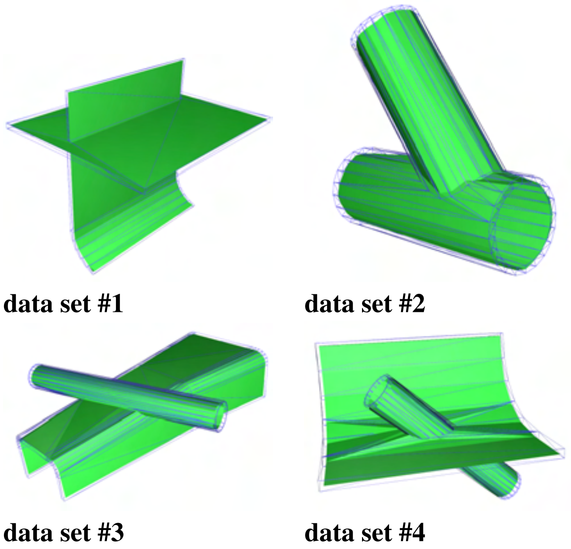

data set #1 data set #2

data set #3 data set #4

Figure 6: This overview shows the input CAD models (wire frame in blue) and the resulting midsurfaces calculated by the vertex climax algorithm (in green).

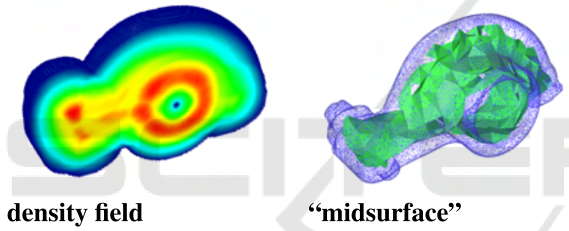

density field "midsurface"

Figure 7: If the input surface geometry is not a thin solid (data set #5), then the accumulated densities (left) do not lead to a directional field that points towards the position of a midsurface. As a consequence the result is undefined.

5 CONCLUSION

A midsurface consists of surface elements (2D) in order to represent three-dimensional, thin solids whose local thickness is small compared to its other dimensions. This important representations allow a significant acceleration of almost all physical simulations. Unfortunately, midsurfaces are not unique and depend on their simulation contexts. Although the creation is a time-consuming, manual step that requires knowledge and experience, it is still the "gold-standard" to speed up a simulation, if FEM can be replaced by thin-shell simulations.

5.1 Contribution

The presented approach to extract a midsurface is applicable to thin-walled parts with a 4-step pipeline consisting of rasterization of the input geometry to obtain a grid-based representation, the generation of a density field using a kernel, moving opposing vertices by a density field to iteratively create a thin representation, and finally a clustering and cleaning step. The first results of this algorithm deliver satisfying results.

5.2 Benefit

The presented approach generates a midsurface without any manual interaction. Only two geometric values (the smallest and the greatest thickness) have to be measured in advance. Once started, no user further interaction is needed. As a consequence, the new approach is suitable for fast feedback loops and rapid prototyping.

5.3 Open Questions & Future Work

The vertex climax algorithm has only one minor issue: the limited precision. The limited precision will be addressed by combining the vertex climax algorithm with an automatic mesh generation algorithm. Having knowledge on the finite element simulation performed on a midsurface allows to limit the discretization artifacts. A locally optimized cell size may prevent additional discretization errors (on top of the mesh generation).

In the future, developments will concentrate on the introduction of local parameters removing the global constants describing the smallest thickness ε, and greatest thickness δ. The goal is to determine these values locally and automatically. In the next step, the influence of these parameters will be examined in more detail.

ACKNOWLEDGEMENTS

The authors would like to thank Ulrich Krispel and Andreas Riffnaller-Schiefer for fruitful discussions; Volker Settgast for providing the input data sets and for his expertise in modeling and construction; Peer Bertram and Martin Schwarz for their expert knowledge in construction and simulation.

REFERENCES

Aichholzer, O. and Aurenhammer, F. (1996). Straight skeletons for general polygonal figures in the plane. *Proceedings of the International Computing and Combinatorics Conference*, 2:117–126.

Demuth, M. and Aurenhammer, Franz und Pinz, A. (2010). Straight skeletons for binary shapes. *Computer Vision* *and Pattern Recognition Workshops (CVPRW)*, 8:9–16.

Fujimori, T., Kobayashi, Y., and Suzuki, H. (2006). Separated medial surface extraction from ct data of machine parts. *Geometric Modeling and Processing*, 4077 (LNCS):313–324.

Itoh, T., Yamaguchi, Y., and Koyamada, K. (1996). Volume thinning for automatic isosurface propagation. *Visualization*, 7:303–310.

Ju, T., Losasso, F., Schaefer, S., and Waren, J. (2002). Dual contouring of hermite data. *ACM Transactions on Graphics*, 21:339–346.

Kazhdan, M., Bolitho, M., and Hoppe, H. (2006). Poisson surface reconstruction. *Symposium on Geometry Processing*, 4:61–70.

Kong, T. and Rosenfeld, A. (1989). Digital topology: Introduction and survey. *Computer Vision, Graphics, and Image Processing*, 48(3):357–393.

Kulkarni, Y. H. (2016). *Development of algorithms for generating connected midsurfaces using feature information in thin walled parts*. PhD Thesis at Savitribai Phule Pune University.

Kulkarni, Y. H. and Kale, M. (2014). Formulating midsurface using shape transformations of form features. *Proceedings of All India Manufacturing Technology, Design and Research*, 5:981–985.

Kulkarni, Y. H., Sahasrabudhe, A., and Kale, M. (2017a). Dimension-reduction technique for polygons. *International Journal of Computer-Aided Engineering and Technology*, 9:1–17.

Kulkarni, Y. H., Sahasrabudhe, A., and Kale, M. (2017b). Leveraging feature generalization and decomposition to compute a wellconnected midsurface. *Engineering with Computers*, 33:159–170.

Kwok, P. C. K. and Ranjan, V. (1991). A survey of 3-d thinning algorithms. *Vision Interface*, 6:13–20.

Lee, T.-C. and Kashyap, R. L. (1994). Building skeleton models via 3-d medial surface/axis thinning algorithms. *Graphical Models and Image Processing (CVGIP)*, 56:462–478.

Lockett, H. and Guenov, M. (2008). Similarity measures for mid-surface quality evaluation. *Computer-Aided Design*, 40:368–380.

Lorensen, W. E. and Cline, H. E. (1987). Marching cubes: A high resolution 3d surface construction algorithm. *ACM SIGGRAPH Computer Graphics*, 21:163–169.

Ma, C.-M. and Wan, S.-Y. (2001). A medial-surface oriented 3-d two-subfield thinning algorithm. *Pattern Recognition Letters*, 22:1439–1446.

Michikawa, T. and Suzuki, H. (2010). Non-manifold medial surface reconstruction from volumetric data. *Geometric Modeling and Processing*, 6130 (LNCS):124–136.

Németh, G., Kardos, P., and Palágyi, K. (2010). Topology preserving 3d thinning algorithms using four and eight subfields. *Image Analysis and Recognition*, 6111:316–325.

Nguyen, Q. T. and Gomes, A. J. P. (2016). Healed marching cubes algorithm for non-manifold implicit surfaces. *Encontro Portugues de Computacao Grafica e Interacao (EPCGI)*, 23:2:1–8.

Nolan, D. C., Tierney, C. M., Armstrong, C. G., Robinson, T. T., and Makem, J. E. (2014). Automatic dimensional reduction and meshing of stiffened thin-wall structures. *Engineering with Computers*, 30:689–701.

Ogayar-Anguita, C.-J., Rueda-Ruiz, A.-J., Segura-Sanchez, R.-J., Diaz-Medina, M., and Garcia-Fernandez, A. L. (2020). A gpu-based framework for generating implicit datasets of voxelized polygonal models for the training of 3d convolutional neural networks. *IEEE Access*, 8:12675–12687.

Palágyi, K. and Németh, G. (2009). Fully parallel 3d thinning algorithms based on sufficient conditions for topology preservation. *Discrete Geometry for Computer Imagery (DGCI)*, 5810 (LNCS):481–492.

Prohaska, S. and Hege, H.-C. (2002). Fast visualization of plane-like structures in voxel data. *IEEE Visualization*, 13:29–36.

Rezayat, M. (1996). Midsurface abstraction from 3d solid models: general theory and applications. *Computer-Aided Design*, 28:905–915.

Schinko, C., Riffnaller-Schiefer, A., Krispel, U., Eggeling, E., and Ullrich, T. (2017). State-of-the-art overview on 3d model representations and transformations in the context of computer-aided design. *International Journal on Advances in Software*, 3 & 4:446–458.

Schinko, C. and Ullrich, T. (2020). A new grid-based midsurface generation algorithm. *Hyperseeing – the Publication of the International Society of the Arts, Mathematics, and Architecture*, 19:81–84.

Schinko, C., Ullrich, T., Schiffer, T., and Fellner, D. W. (2011). Variance Analysis and Comparison in Computer-Aided Design. *Proceedings of the International Workshop on 3D Virtual Reconstruction and Visualization of Complex Architectures*, XXXVIII-5/W16:3B21–25.

Shawn, M. and Watson, J.-P. (2011). Non-manifold surface reconstruction from high-dimensional point cloud data. *Computational Geometry*, 44:427–441.

Sun, L., Tierney, C. M., Armstrong, C. G., and Robinson, T. T. (2016). Automatic decomposition of complex thin walled cad models for hexahedral dominant meshing. *Procedia Engineering*, 163:225–237.

Toriwaki, J. and Yonekura, T. (2002). Euler number and connectivity indexes of a three dimensional digital picture. *Forma*, 17:183–209.

Ullrich, T., Settgast, V., and Fellner, D. W. (2008). Abstand: Distance Visualization for Geometric Analysis. *Project Paper Proceedings of the Conference on Virtual Systems and MultiMedia Dedicated to Digital Heritage (VSMM)*, 14:334–340.

Woo, Y.-H. and Choo, C.-U. (2009). Automatic generation of mid-surfaces of solid models by maximal volume decomposition. *Transactions of the Society of CAD/CAM Engineers*, 14:297–305.

Yamzaki, S., Kae, K., and Ikeuchi, K. (2002). Non-manifold implicit surfaces based on discontinuous implicitization and polygonization. *Geometric Modeling and Processing*, 12:138–146.